Full Paper Transactions, SMiRT 28
Toronto, Canada, August 10-15, 2025

AN INVESTIGATION OF THE RSE-M CRACK CLOSURE PARAMETER F(R) ON AN AUSTENITIC PWR COMPONENT WITH NEGATIVE R-RATIO INCLUDING WELDING RESIDUAL STRESS

Mike P Nielsen[1]

[1] Technical Director, Kinectrics UK, Altrincham, Cheshire, UK (mike.nielsen@kinectrics.com)

ABSTRACT

This paper provides an investigation of the crack closure parameter, f(R) in the RSE-M code for a representative austenitic pressurised water reactor component where the main loading arises from pressured thermal transients. The primary focus is the treatment of the start-up/shutdown transients, initially giving rise to a (elastically) negative R-ratio, subsequently modified by the inclusion of welding residual stress. Consideration is also given to on-load variations (with positive R-ratio and small ΔK) to illustrate the effects of load history and crack closure. The analysis has shown that cases including WRS which result in a change from negative to positive R-ratio when determined using the conventional codified route were confirmed to be negative in the region of the crack-tip, and indeed significantly so ahead of the crack. Whilst, on first inspection, this may seem like a significant source of conservatism in the codified route, the expressions used to determine ΔK_{eff} are derived from data without WRS. The work here is limited to determination of R-ratios for use on existing f(R) formulations only, and reporting ΔK_{eff} determined directly from the models is expected as part of future work. However, it confirms the suitable accuracy of the codified f(R) formulation for cases with no WRS. Potential alleviation via sensitivity cases in structural assessments of austenitic components in cases containing WRS proposed.

INTRODUCTION

Operation of a civil nuclear PWR facility results in a complex variable loading sequence arising from combined mechanical and thermal loadings, in additional to welding residual stresses. This presents a challenge for structural assessments at the design stage (no load history) in support of a safety case of components for which gross failure must be shown to be incredible within the design life.

In the UK, fracture mechanics assessments (FMA) are used as part of the substantiation of the components requiring the highest reliability claims, referred to as high integrity components (HICs). A demonstration via FMA is required to show that a defect size margin (DSM) approaching 2.0 can be achieved. The DSM is defined as:

$$DSM = \frac{ELLDS}{QEDS+FCG} \cong 2 \quad (1)$$

The UK FMA demonstration postulates defects at the design stage. However, the assessment methods for FCG are based on in-service inspection codes such as ASME XI or RSE-M. The study here focuses on the methods in RSE-M. However, in general, the goal of any in-service inspection code is to justify continued operation by sentencing of defect, typically to the next inspection interval (~10 years). Assessments of any defect found in-service have the advantage of known operating history, at least in terms of numbers of cycles/transient occurrences. Conversely, the exact history of the formation of the defect has less certainty. Therefore, when these factors are taken into account, the use of conservative assessment methods and/or material behaviour still results in acceptable outcomes in terms of continued operation.

Modern computing capabilities enable analysis of components in much greater detail than was possible for the earlier generations of plant designs using the same or similar technology. Detailed analysis results are increasingly indicating risks in terms of guarding against some relevant failure mechanisms not identified in previous design assessments, or apparent in generating plant OPEX. Some notable factors for this can be attributed to; methods which have not developed at the same rate as the analysis techniques (often due to lack of necessity), conservative materials data/behaviour from tests significantly older than the plant under assessment, or a combination of the two.

The motivation for the work here is to better understand the relative contribution of aspects of the fatigue crack growth (FCG) assessment route to assist with making judgments in structural assessments where high FCG is predicted using the readily available existing tools. The overall aim is to develop more accurate estimation of ΔK_{eff} in routine structural assessments of large components subjected to pressurised thermal transients. This paper presents an initial study focussing on the crack closure parameter, f(R) in the RSE-M code (AFCEN, 2018) in the case of representative austenitic components to highlight how aspects such as plasticity and load symmetrisation impact the R-ratio. The primary focus is the treatment of the start-up/shutdown transients initially giving rise to (elastic) negative R-ratios, subsequently modified by the inclusion of welding residual stress. Consideration is also given to on-load (normal operating) variations (with positive R-ratio and small ΔK) to illustrate the effects of load history and crack closure. It follows similar work by the Author on ferritic components (Nielsen, 2024), though the work here considers two geometries under the same combined pressure and thermal loading; in one case the elastic thermal loading is dominant, and in the other the thermal and pressure loading are similar. For each geometry the influence of welding residual stress is also considered.

Appendix 5.6 of RSE-M defines the FCG rate in terms of crack growth per cycle, da/dN. For austenitic forgings, welds and castings in a PWR water environment, the FCG rate laws (derived using compact test specimens) are provided in Table 5.6-II.2. Crack growth, da/dN is determined as follows:

$$\frac{da}{dN} = C\left(\Delta K_{eff}\right)^n \tag{2}$$

$$\Delta K_{eff} = f(R)\Delta K_{cp} \tag{3}$$

$$R = \frac{K_{min}}{K_{max}} \tag{4}$$

The general form of the f(R) parameter for austenitic materials depends on the sign of K_{min} and the material. If $K_{min} \geq 0$, f(R) is determined from:

$$f(R) = \frac{1}{1-R/2} \tag{5}$$

If $K_{min} < 0$, f(R) is determined from Equation 5 using a negative R-ratio, with a minimum value of 1/3. For completeness, in the case that K_{max} is also negative, f(R) is fixed to a value of 1/3. A range of f(R) values between R of -4 to 1 are presented in Figure 1. The expression for f(R) in Equation 5 is based on work from Rabbe and Lieurade (1972).

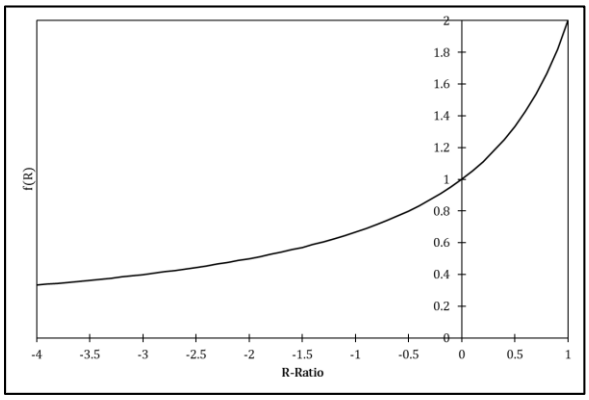

Figure 1. Variation of RSE-M Crack Closure Parameter, f(R), with R-Ratio for Austenitic Forgings and Welds

A notable issue with detailed analyses of FCG in the components considered here is obtaining a reliable estimate of ΔK_{eff} from the numerical model. There is a lack of readily available large-scale test results under representative loading conditions. Therefore, it is necessary to attempt to rationalise results against classical theory and/or small-scale laboratory experimental evidence as appropriate. Work is ongoing by the Author to investigate methods of obtaining ΔK_{eff} from numerical analyses with more reliability for use in routine structural assessments. The work here forms an initial part of this goal, and in the interest of clarity will be limited to presentation of R-ratios obtained from the models for comparison with those determined via the codified route. These will then be used to infer potential impacts to f(R) using the relationship illustrated in Figure 1, given by Equation 5.

MODELLING

Axisymmetric models of two cylindrical geometries with $r_i/t_w \sim 5$, lengths > 5 diameters, with and without a 10mm deep circumferential defect have been constructed using ABAQUS finite element software (Dassault, 2021). The defect is modelled with a 10μm root radius, which is judged to be more representative for an austenitic material with larger grain sizes. An analytical rigid plane is also included to prevent over-closure of the crack face under compressive loading.

The initial focus for the work here was high calculated growth on a large cast component. Thus, the larger of the two geometries is intended to be representative in terms of through-wall dimensions of the cast component. The smaller geometry has dimensions more representative of pipework components. However, to reduce the number of variables between the two sets of analyses to aid comparisons, properties for a cast material have also been assumed. The larger diameter model has an internal radius of 1,000mm and a wall thickness of 200mm. The smaller diameter model has an internal radius of 380mm, and a wall thickness of 76mm. The 200mm model is shown in Figure 2. Note that in all cases (200mm and 76mm), the same cracked part was used and tied to the respective remainder of the geometry.

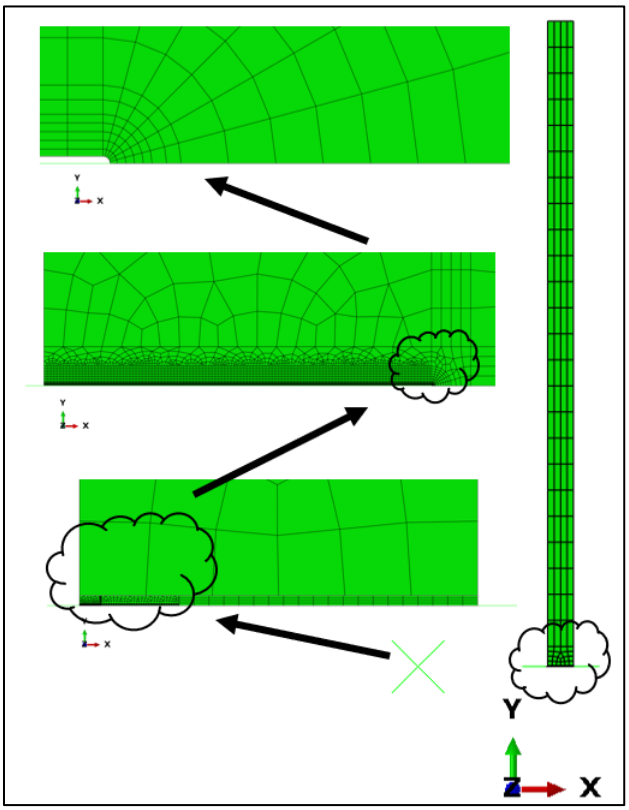

Figure 2. Example Finite Element Model Used Showing Details of Cracked Part Containing 10mm Deep Defect

Heat transfer and stress analyses were carried out. For the un-cracked analyses sequential heat transfer and stress analyses were performed. For the cracked-body analyses, coupled analyses were used with adaptive meshing techniques in the region of the crack-tip. In all cases, a large constant HTC value has been assumed throughout the analysis. This is representative for PWR normal operating conditions when flow rates are high, though less so for some parts of the start-up or shutdown cycle. However, for the purposes of the study here, the assumption is judged reasonable.

The component is assumed to be constructed from cast austenitic stainless steel, Type Z3 CN 20-09M (similar to AISI 304). Elastic tensile and physical properties have been taken from Appendix Z I of RCC-M at 20°C and 350°C. Monotonic true stress-strain data are taken from Tables 5.6.III.3-9 and 10 in Appendix 5.6 of RSE-M. The use of monotonic curves is judged reasonable on the basis that there are fewer than 100 major stress (start-up/shutdown) cycles in the design life of the components considered here, thus fully stabilised cyclic behaviour is not expected.

Analyses have been carried out assuming elastic, elastic perfectly plastic, non-linear isotropic and mixed hardening behaviours. Mixed hardening has been carried out using the non-linear hardening options in ABAQUS, with Chaboche parameters obtained according to Kalnins et al. (2015). It should be noted that the aim of the analyses here is not to provide definitive values in terms of damage, but to illustrate trends. The importance of material hardening models and associated uncertainty in finite element applications is noted and results from all analyses are not presented here, though some general conclusions are provided later.

The loading is defined in more detail later. However, as in Nielsen (2024), to set the logic for the cases considered the part of the plant operating condition POC cycle analysed in detail is the shutdown/start-up operation. In the components considered here, start-up operations result in heating transients, giving rise to compressive stresses on the internal surface, resulting in a negative R-ratio. Consideration of the influence of welding residual stress (WRS) leads to the following cases to be analysed:

1. Negative R-ratio, no WRS.
2. R-ratio enhanced by WRS.

Case 1 is the base case and representative of assessments carried out on parent materials. Case 2 is representative of a non-PWHT welded component for which inclusion of tensile WRS results in a positive K_{min}. WRS are not cyclic but contribute to the mean stress. This is accounted for by a modification to Equation 4, and R-ratios for Case 2 are determined using Equation 6:

$$R^* = \frac{K_{min}+K_{res}}{K_{max}+K_{res}} \tag{6}$$

Again, as described in Nielsen (2024), the major stress cycles generally occur due to thermal transients associated with normal shutdown and start-up operations. A period of fictious continuous operation has been defined, which includes an initial start-up, a period of steady operation followed by a shutdown, and then repeated (Figure 3). The total period considered for one cycle of continuous operation is approximately 61 hours. For analysis purposes, the period of the start-up transient has been optimised to reduce analysis run time. In practice, the temperature is held constant at ~15°C for several hours at low pressures while the main coolant pumps are brought into service. This period is omitted from the analyses and the transient is assumed to begin as pumps are started and the pressure is increased, resulting in a rapid temperature change from 20°C to 50°C

Approximate WRS distributions have been determined from a thermal analysis of an arbitrary cooldown transient, obtained via an elastic thermal analysis on an uncracked model with an undeformed mesh (displacements not written to the ABAQUS *.odb file). The ABAQUS *initial conditions, TYPE=STRESS was used to introduce an initial stress state. A dummy static step was then run to obtain equilibrium to achieve a self-balancing stress distribution with representative values close to the inside surface. This is reasonable on the basis that the scope here relates to small defects in thick section components. The time step was chosen to ensure magnitudes over the depth of the defect of approximately 100% of the room temperature (lower bound) yield stress. This is reasonable and conservative for components not subject to post-weld heat treatment.

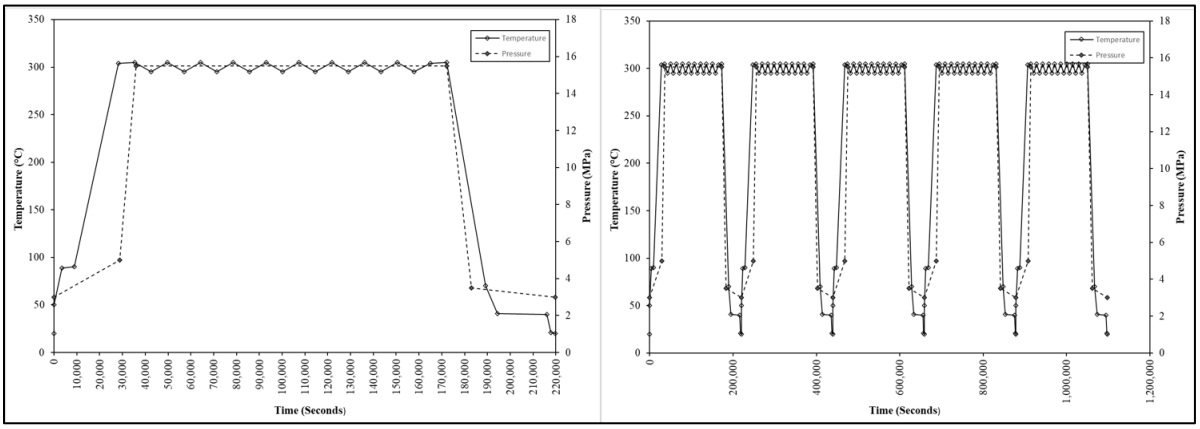

Figure 3. Loading Profile, Single POC Cycle (Left) and 5 Cycles (Right)

RESULTS

The analyses for both 200mm and 76mm geometries have been assessed as follows:

- Step-1: Determine ΔK_{eff} from an un-cracked elastic analysis using f(R) from RSE-M.
- Step-2: For each elastic and elastic-plastic analysis obtain stress-strain hysteresis loops at a characteristic length ahead of the crack-tip.
- Step-3: Use the output from Step-2 to infer an R-value.
- Step-4: Compare R-values from the models with those from the codified elastic route to infer f(R).

Note that Opening (perpendicular to crack) stresses and von Mises stress ahead of the crack-tip, reaction forces on the un-cracked ligament and crack face displacements have also been reviewed but are not reported here for brevity and will form part of the next phase of work.

Combined elastic thermal and pressure stresses at a point 10mm below the surface in the case with no WRS are shown in Figure 4. Through-wall stress distributions have been extracted at the time of the maximum (shutdown) and minimum (start-up) stresses for an assessment of Cases 1, 2 and 3. K_{max}, K_{min} and K_{res} values have been derived using influence functions for an internal axisymmetric defect from Chapter VII.2.2.3 in Appendix 5.4 of RSE-M (solution "TUB-CDAI") to determine ΔK. The R-ratio has been determined using Equation 4 and 6 as appropriate, and f(R) using Equation 5. The results for Cases 1 and 2 are presented in Table 1.

TABLE 1 Un-Cracked Elastic Assessment Results, Depth a = 10mm

Parameter	Units	Case 1a (200mm model No WRS)	Case 1b (76mm model No WRS)	Case 2a (200mm model +WRS)	Case 2b (76mm model +WRS)
$K_{I\,max}^{tot}$	MPa√m	44.8	5.6	As Case 1a	As Case 1b
$K_{I\,min}^{tot}$	MPa√m	-30.4	-7.4		
ΔK_I^{tot}	MPa√m	75.2	13.0		
K_I^{res}	MPa√m	0.0	0.0	41.5	16.1
R	-	-0.678	-1.331	0.129	0.400
$f(R)$	-	0.747	0.600	1.069	1.250
ΔK_{eff}	MPa√m	56.2	7.8	80.4	16.3

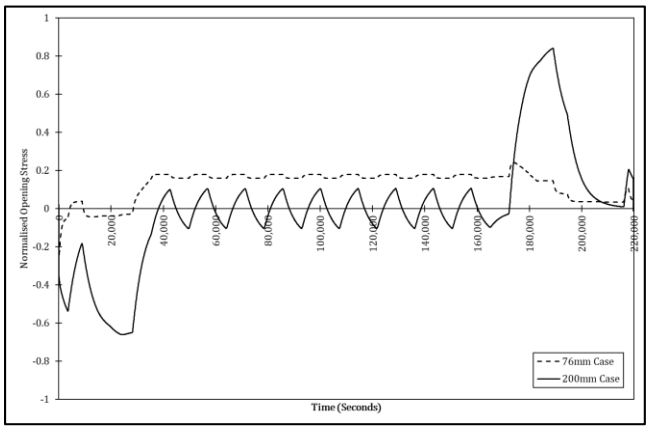

Figure 4. Un-Cracked Elastic Axial Stress 10mm Below Surface

Cracked-Body Analysis – 200mm Cases

The elastic stress-stain hysteresis loops with, and without WRS at 59µm ahead of the crack-tip are shown in Figure 5(a). The start of the cycle is shown by the solid star, and the direction with the thick arrow shapes. The distance of 59µm is the "characteristic length", d, recommended for determination of stress range in fatigue crack initiation assessments in Appendix 5.6 of RSE-M. The R-ratios from the maximum and minimum stresses are 0.064 and -0.667, with and without WRS respectively. For the elastic-plastic cases. The hysteresis loops from the 5th cycle are shown in Figure 5(b). Again, the start of the cycle is shown by the solid star, and the direction with the thick arrow shapes. The R-ratios from the maximum and minimum stresses are -0.864 and -0.804, with and without WRS respectively. Symmetrisation of the cycle is immediately evident compared to the elastic case. The large translation of the case with WRS is due to triaxial effects, noting that the traces here comprise only the axial stress-strain component.

It is noted that the determination of R-ratio here is from the stress-range at a single point ahead of the crack-tip. In the elastic case, there is excellent agreement with the R-ratio determined using influence function coefficients and Equation 4. However, as an additional check reaction forces on the remaining un-cracked ligament have been checked in the elastic and elastic-plastic cases without WRS to investigate the R-ratio. In the elastic case the R-ratio is reasonably constant at approximately -0.672 to a depth a/t = 0.25. The 5th cycle in the elastic-plastic case shows slightly more variation, but an average R-value of -0.878 to a depth a/t = 0.25. For reference, the average R-value for the 1st and 2nd cycles, over the same depth, is approximately -1.2. Comparing values from the elastic and elastic-plastic 5th cycle to those obtained from the hysteresis loops, shows good agreement for the elastic case and reasonable agreement elastic-plastic case. Overall, the additional check provides sufficient confidence that R-ratios obtained from the stress-strain hysteresis loops can be used to infer R-values determined using an influence function approach.

From the above analysis, it can be seen that in the elastic case with no WRS there is good agreement between the codified R-value (Equation 4), stress-strain hysteresis loops and reaction forces. The elastic case with WRS shows that the modified R-value (Equation 6) would lead to a notably higher value of ΔK_{eff} compared to that determined from the stress-strain hysteresis loop. The elastic-plastic analyses both with and without WRS, result in negative R-ratios from both the hysteresis loops and the reaction forces.

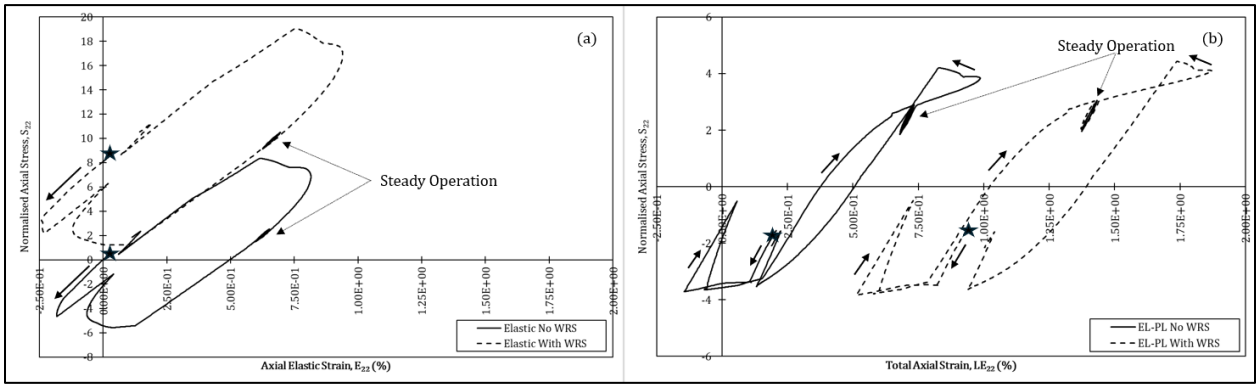

Figure 5. 200mm Geometry Elastic and Elastic-Plastic Stress-Strain Hysteresis Loops at 59µm

Cracked-Body Analysis – 76mm Cases

The elastic stress-stain hysteresis loops with, and without WRS at 59µm ahead of the crack-tip are shown in Figure 6(a). Again, the start of the cycle is shown by the solid star, and the direction with the thick arrow shapes. The R-ratios from the maximum and minimum stresses are 0.413 and -0.851, with and without

WRS respectively. The elastic-plastic hysteresis loops from the 5th cycle are shown in Figure 6(b). Again, the start of the cycle is shown by the solid star, and the direction with the thick arrow shapes. The R-ratios from the maximum and minimum stresses are -0.937 and -1.231, with and without WRS respectively. Similar conclusions regarding symmetrisation of the loops, and translation of the elastic-plastic WRS case made for the 200mm geometry also apply.

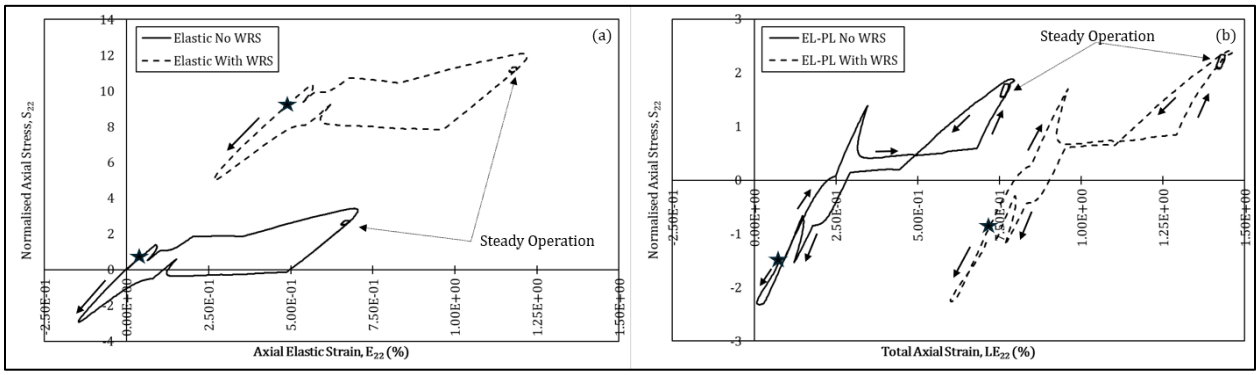

Figure 6. 76mm Geometry Elastic and Elastic-Plastic Stress-Strain Hysteresis Loops at 59µm

DISCUSSION

The work here has purposely avoided estimates of ΔK_{eff} from the finite element models, though this is the goal of future work. Whilst several detailed methods are readily available using numerical methods, such as ΔJ, these are also not without limitation. For example, Li et al. (2019), present a method for determination of ΔJ using finite element analysis, referred to as the "quarter-cycle" method. However, to remain within the validity of the J-integral formation, the cycle is modified such that the range is applied as a monotonic increasing load. The resulting ΔJ is converted elastically back to ΔK, and the remainder of the codified route is followed, including the determination of ΔK_{eff} using Equation 3. In this respect the quarter-cycle ΔJ approach, although more accurate and reasonably convenient to employ in practice, still does not rationalise the codified f(R), Equation 5 in this case.

Watson et al. (2015) proposed several formulations for the f(R) function (referred to as q_0 in their work) based on testing of small Type 304 cylindrical specimens in air at 260°C under displacement-controlled loading. Testing was extended to PWR environments by Pellereau et al. (2020). The outcomes were revised expressions for q_0 though the overall form remains consistent with that proposed by Rabbe and Lieurade (1972). Recommended and best estimate expressions were derived based on "elastic" and "non-elastic" conditions. The latter are defined as those with applied strain ranges greater than ±0.2%. For the 200mm geometry, the elastic-plastic strain ranges are 1.7% and 1.2% with and without WRS respectively (Figure 5(b)). For the 76mm geometry, the elastic-plastic strain ranges are 0.9% and 0.8% with and without WRS respectively (Figure 6(b)). Therefore, both geometries correspond to the "non-elastic" conditions. For these conditions, Watson et al. (2015) provided the following for bounding and best estimate use, reproduced here as Equations 7 and 8 respectively. Equation 8 is intended for benchmarking only, and not for use in structural assessments, though is considered most appropriate in the comparisons here.

$$q_0 = max\left\{\frac{1}{3}, \frac{1}{1-R/3}\right\} \tag{7}$$

$$q_0^{BE} = \frac{1}{1-R/1.734} \tag{8}$$

Although, Equations 7 and 8 represent an example of recent and relevant work providing some further basis to Equation 5, the loading is not exactly representative of that of the plant, discussed further below. Nevertheless, they are considered suitable to provide initial conclusions, and some level of semi-quantification of the overall trends observed from study here. Results for both the 200mm and 76mm geometries are plotted together in Figure 7 fitted to the resulting curve from Equation 5. The figure also includes the curves from Equations 7 and 8. It can be seen that for both geometries, with and without WRS, the elastic-plastic R-ratios are negative with an average value of approximately -0.95. The negative R-values in the cases with WRS is due to symmetrisation of the loading cycle, which in the work here occurs at the start of the analysis.

An indication of the impact of the elastic-plastic results on ΔK_{eff} can be obtained by translating the R-values to the curves of Equations 7 and 8. For example, in the 200mm case with no WRS, Equation 7 leads to an increase of f(R) of ~5.6%, whist Equation 8 gives a reduction of ~8.5%. The same exercise for the case with WRS results in reductions to f(R) of approximately 27.4% and 37.6% for Equations 7 and 8 respectively. However, the latter results are heavily caveated by the fact that the under-pinning work by Watson et al. (2015) did not include cases with residual stress.

As noted earlier, the purpose of this paper was not to draw full conclusions or make definitive recommendations at this stage. There are, however, some aspects judged noteworthy for consideration in structural assessments. Firstly, the representativeness of small-scale tests, conservative or otherwise, is difficult to reliably quantify. Although displacement-controlled testing can be carried out at elevated temperatures, some effects are not captured such as the stiffness effects associated with the change of temperature and Young's modulus. This is prominent in the 200mm case (Figure 5) where the stress continues to increase while the strain decreases during the shutdown part of the cycle. It should be noted that normalisation of the stresses/stress-strain hysteresis loops (Figures 4, 5 and 6) has been done using the room temperature 0.2% yield stress (207 MPa). The work hardened yield stresses at the strain ranges presented here are notably higher, although plastic accommodation is still not expected.

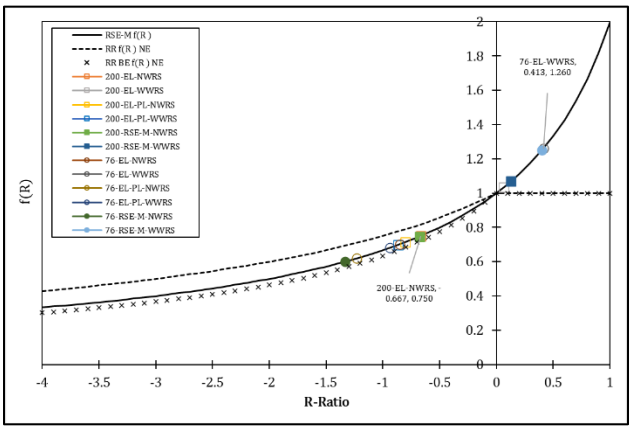

Figure 7. R-Ratios from Analyses Fixed to the Curve of Equation 5

Taking the above aspects into account with the results in Figure 7, the use of Equation 5 is considered suitably accurate i.e. not overly conservative, for structural assessments of components with no WRS. There is insufficient information from the study here to draw definitive conclusions regarding cases with WRS, despite the "favourable" R-ratios, although Equations 5 and 6 are expected to be very conservative. In addition, the cautionary observations in Nielsen (2024) regarding simplified component

and defect geometry and the effect on triaxiality of introducing WRS by imposed thermal field into a model are reiterated here.

Significantly noteworthy observations for both geometries are the load history effects and the subsequent positioning of the normal operating variations. The large thermal variations associated with the start-up/shutdown part of the cycle dominate, even in the 76mm geometry. From Figure 3, the normal operating variations could be considered as positive R-ratio sub-cycles within the start-up/shutdown cycles. In practice, these types of cycles large numbers of design cycles and when considered in isolation make up a significant proportion of the overall FCG. However, inspection of Figures 5 and 6 suggest that these cycles have no impact to the overall stress or strain ranges. There is a need to ensure that all faults considered in the design basis are adequately accounted for in design stage structural assessments. Attempts to refine transient schedules/design inputs to reduce over-conservatisms, if possible, requires consideration of several stakeholders to ensure that unnecessary burden is not transferred to the operator. If required, in the first instance, given the observations here it is judged reasonable to account for potential excessive conservatisms in design inputs and/or assessment routes in industrial applications of cases with WRS, via sensitivity cases. For example, to determine FCG arising from the start-up/shutdown cycles only with R determined from Equation 6. It is strongly emphasised that this type of exercise requires user justification based on a full appreciation of all the design transients and loading on a case-by-case basis.

CONCLUSION

An initial investigation of the RSE-M crack closure parameter, f(R), for austenitic components has been performed using results generated from elastic-plastic cracked body finite element analyses of two geometries representative of large PWR primary circuit components.

The analysis has shown that cases including WRS which result in a change from negative to positive R-ratio when determined using the conventional codified route were confirmed to be negative in the region of the crack-tip, and indeed significantly so ahead of the crack. Whilst, on first inspection, this may seem like a significant source of conservatism in the codified route, the expressions used to determine ΔK_{eff} are derived from data without WRS. Furthermore, the work here is limited to determination of R-ratios for use on existing f(R) formulations only, and reporting ΔK_{eff} determined directly from the models is expected as part of future work.

The work confirms the suitable accuracy of the codified f(R) formulation for cases with no WRS e.g. assessments carried out in base metal locations. In addition, the impact of the on-load (normal operating) variations has been observed and potential alleviation via sensitivity cases in structural assessments of austenitic components in cases containing WRS proposed.

NOMENCLATURE

C	=	intercept constant on the log-log FCG rate curve
ΔK_{cp}	=	elastic stress intensity factor range with confined plasticity correction
ΔK_{eff}	=	effective stress intensity factor range
d	=	characteristic length for low alloy steel material, taken as 50μm
ELLDS	=	end-of-life limiting defect size
FCG	=	fatigue crack growth
K_{max}	=	maximum elastic stress intensity factor
K_{min}	=	minimum elastic stress intensity factor
OPEX	=	operation experience

n	=	slope of the log-log FCG rate curve (in region II)
POC	=	plant operating condition
QEDS	=	qualified examination defect size
ri	=	internal radius
t_w	=	wall thickness

ACKNOWLEDGMENTS

The author wishes to thank Antony Hurst and Fraser Barber from Kinectrics UK, and Alex Mann from EdF Energy for their support and contribution to the work in this paper.

REFERENCES

AFCEN. (2018). *"*In-Service Inspection Rules for Mechanical Components of PWR Nuclear Islands*", RSE-M 2018 Edition.*

Dassault – ABAQUS 2021.

Kalnins, A., Rudolph, J., Willuweit, A. (2015). "Using the Nonlinear Kinematic Hardening Material Model of Chaboche for Elastic-Plastic Ratcheting Analysis," *Journal of Pressure Vessel Technology*, Volume 137, June 2015.

Li, J., Ancelet, O., Double, A., Chapuliot, S. (2019). "Evaluation of Fatigue Crack Propagation by ΔJ Approach", *Proceedings of the ASME 2019 Pressure Vessels & Piping Conference, PVP2019-93555, July 14-19, San Antonio, TX, USA.*

Nielsen, M. P. (2024). "An Investigation of the RSE-M Crack Closure Parameter f(R) on a Large Ferritic PWR Component with Negative R-Ratio including Welding Residual Stress*". Proc. 9th Engineering Integrity Society International Conference of Durability and Fatigue (Jesus College, Cambridge UK, June 2024) 2024; 2:506–519.*

Pellereau, B., Currie, C., Mann, J. (2020). "Investigation into Crack Closure Effects for Fatigue Crack Growth Under Negative R Conditions*", Proceedings of the ASME 2020 Pressure Vessels & Piping Conference, PVP2020-21627, August 3, Virtual, online*.

Rabbe, P. and Lieurade, H. P. (1972). "Etude a l'aide de la méchanique de la rupture de la Vitesse de fissuration en faigue d'une gamme etendue d'aciers," (Translated "*Study of Fatigue Crack Growth Rates of a Wide Range of Steels using Fracture Mechanics*"), Memoires Scientifiques, Rev. Métallurgie, 69, No. 9, Revue de la Métallurgie S. A., Paris.

Watson, C., Currie, C., Emslie, J. (2015). "Accounting for Negative R-Ratio (Crack Closure) in Fatigue Crack Growth Calculations of Stainless-Steel Components*", Proceedings of the ASME 2015 Pressure Vessels & Piping Conference, PVP2015-45622, July 19-23, Boston, Massachusetts, USA.*